Spectacular Doping Dependence of Interlayer Exchange and Other Results on Spin Waves in Bilayer Manganites

T. G. Perring,[1] D. T. Adroja,[1] G. Chaboussant,[1] G. Aeppli,[2] T. Kimura,[3] and Y. Tokura[3,4]

[1]*ISIS Facility, CLRC Rutherford Appleton Laboratory, Didcot, Oxon OX11 0QX, United Kingdom*

[2]*NEC Research Institute, 4 Independence Way, Princeton, New Jersey 08540*

[3]*Department of Applied Physics, University of Tokyo, Tokyo 113-8656, Japan*

[4]*Joint Research Center for Atom Technology (JRCAT), Tsukuba 305-0046, Japan*

(Received 14 May 2001; published 31 October 2001)

We report the measurement of spin waves in the bilayer colossal magnetoresistive manganites $La_{2-2x}Sr_{1+2x}Mn_2O_7$ with $x = 0.30$, 0.35, and 0.40. For $x = 0.35$ and 0.40 the entire acoustic and optic dispersion relations are well described by those for a bilayer Heisenberg Hamiltonian with nearest-neighbor exchange only, which is explained together with the spin-wave lifetimes by the double exchange model. The in-plane exchange depends weakly on x, but that between the planes of a bilayer changes by a factor of 4, directly revealing a change from mixed $d_{3z^2-r^2}$ and $d_{x^2-y^2}$ orbital character to mostly $d_{x^2-y^2}$.

DOI: 10.1103/PhysRevLett.87.217201 PACS numbers: 75.30.Vn, 75.30.Ds, 78.70.Nx

The cubic manganese perovskites $R_{1-x}A_xMnO_3$ (R = La, Nd, Pr, A = Sr, Ca, Pb, for example) have attracted attention because of their rich and fascinating physical properties. These can include not only changes in resistivity of several orders of magnitude in an applied field of a few tesla, but also magnetic field, electric field-, photon-, and strain-induced insulator-to-metal phase transitions [1]. The starting point to understanding the manganites is double exchange (DE) theory [2,3] in which electrons in partially filled e_g bands hop between adjacent Mn ions, each of which has a spin $S = 3/2$ arising from local t_{2g} orbital occupancy. Strong intrasite exchange $J_H \sim 2$ eV favors hopping between parallel Mn spins and therefore ferromagnetism and metallic conductivity. DE alone cannot explain the physics of the manganites, however, and there is a wealth of evidence pointing towards lattice distortions which localize carriers to form polarons in the paramagnetic phase [4].

Naturally layered manganites [5] allow the influence of another control parameter, that of dimensionality, to be explored. In addition, they provide the venue for an object not found elsewhere in nature, namely a two-dimensional, fully spin-polarized electron liquid. $La_{2-2x}Sr_{1+2x}Mn_2O_7$ consists of bilayer slices of MnO_6 octahedra taken from the cubic compound, separated by insulating $(La, Sr)_2O_2$ layers that serve to largely decouple the bilayers both electronically and magnetically [Fig. 1(a)]. The influence of reduced dimensionality is seen in the enhanced CMR near the three-dimensional ordering temperature T_C as compared to the cubic $(La, Sr)MnO_3$ analog, albeit at the cost of reduced $T_C \sim 100-120$ K [5].

Surprisingly, there are very few results for the spin waves in bilayer manganites [6–8]. Published work is confined to just $x = 0.4$, with only one preliminary report of measurements to the zone boundary [8], and no quantitative analysis of the spin-wave lifetimes as a function of momentum. Here we present the results of a study as a function of hole doping in the range $x = 0.30-0.40$. We show that the interplane (but still intrabilayer) coupling shows a remarkable sensitivity to hole doping, which is explained by changing $d_{3z^2-r^2}$ orbital occupancy, and that for $x = 0.35$ and 0.40 the spin waves throughout the Brillouin zone can be understood fully within the framework of the DE model.

Our neutron scattering data were taken for single crystals of $La_{2-2x}Sr_{1+2x}Mn_2O_7$ with masses 0.7, 2.9, and 1.9 g for $x = 0.30$, 0.35, and 0.40, respectively. Neutron diffraction confirmed that the moments in the ordered phases are ferromagnetically ordered within the bilayers [9–12]. For $x = 0.35$ and 0.40 the bilayers have weak ferromagnetic coupling to neighboring bilayers resulting in Curie temperatures, T_C, of 118 and 120 K, respectively, while for $x = 0.30$ the coupling is antiferromagnetic, $T_N = 90$ K. In this paper, we are concerned only with *intrabilayer* coupling; in fact *interbilayer* coupling is unmeasurable in these experiments, being ~100 times smaller [13]. The spin-wave measurements were performed at $T \approx 10$ K $\ll T_C$ or T_N on the HET and MARI spectrometers of the ISIS pulsed neutron source at the Rutherford Appleton

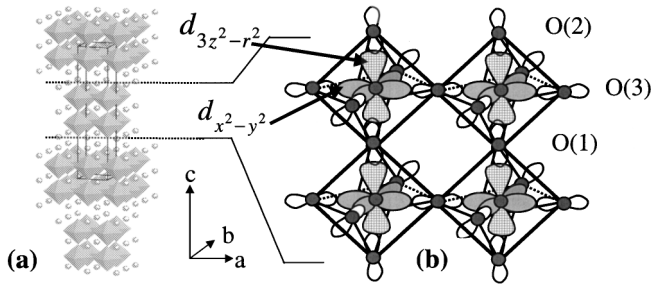

FIG. 1. (a) Crystal structure of $La_{2-2x}Sr_{1+2x}Mn_2O_7$. The Mn ions are at the center of the MnO_6 octahedra. Circles denote La and Sr. (b) Expanded view of MnO_6 octahedra in a single bilayer, showing the Mn $d_{3z^2-r^2}$ and $d_{x^2-y^2}$ orbitals.

Laboratory, U.K. [14]. From just a few choices of incident energy and crystal orientation the entire dispersion relation along the major symmetry directions could be mapped out for $x = 0.35$ and $x = 0.4$. With the smaller $x = 0.30$ crystal data could be obtained only near the zone center.

To analyze the data we considered the Hamiltonian for a Heisenberg ferromagnet (HFM) with coupling J_{ij} between localized spins at sites i and j, $H = -\sum_{\langle i,j\rangle} J_{ij}\mathbf{S}_i \cdot \mathbf{S}_j$. The simplest form of the Hamiltonian is when there are only nearest-neighbor interactions (nnHFM): $J_\parallel$ along Mn-O-Mn bonds in the plane and $J_\perp$ along Mn-O-Mn bonds that connect the two planes of a bilayer. Applying linear spin-wave theory of the Holstein-Primakoff type [15] yields acoustic and optic spin-wave dispersion relations $\hbar\omega_{\rm ac}(\boldsymbol{Q}) = 4SJ_\parallel[\sin^2(Q_x a/2) + \sin^2(Q_y a/2)]$ and $\hbar\omega_{\rm op}(\boldsymbol{Q}) = \hbar\omega_{\rm ac}(\boldsymbol{Q}) + 2SJ_\perp$ (here $a = 3.86$ Å), and the neutron scattering cross section per Mn site

$$\frac{d^2\sigma}{d\Omega\, d\omega} = \left|\frac{k_f}{k_i}\right|(\gamma_N r_0)^2 \frac{S_{\rm eff}}{2}|F(Q)|^2[1 + (Q_z/Q)^2][\cos^2(Q_z\Delta z/2)S^{\rm ac}(Q,\omega) + \sin^2(Q_z\Delta z/2)S^{\rm op}(Q,\omega)],$$

where $S^{\rm ac,op}(Q,\omega) = (n_\omega + 1)\delta[\omega - \omega_{\rm ac,op}(Q)] + n_\omega\delta[\omega + \omega_{\rm ac,op}(Q)]$, with $n_\omega = (1 - e^{-\beta\hbar|\omega|})^{-1}$ and $\Delta z = a$ to 2%. Here $F(Q)$ is the magnetic form factor and $(\gamma_N r_0)^2$ is 291 mbarns/sr. The possibility of finite spin-wave lifetimes was allowed for by replacing the delta-function response with that for a damped simple harmonic oscillator with inverse lifetime γ. To place points on the acoustic dispersion relation, each spin wave with integer $Q_z\Delta z/2\pi$ was fitted to the convolution of the neutron scattering cross section and the instrument resolution. The optic spin-wave dispersion relation was established by using the previously determined acoustic dispersion to derive an effective $J_\perp$ for each spin wave with half-integer $Q_z\Delta z/2\pi$. In this fashion, each acoustic and optic spin-wave peak was independently assigned a position on the dispersion relation, an intensity, and a lifetime. The results are summarized in Figs. 2 and 3.

We consider first the dispersion relations for $x = 0.35$ and $x = 0.40$, shown in Fig. 2. The principal features are that well-defined spin waves exist to at least 70 meV, and that there is no softening of the branches near the zone boundary. Solid lines show the best fits to the data for the nearest-neighbor Heisenberg Hamiltonian. Except near the $(1/2, 0)$ zone boundary for the optic branch, the model provides a reasonably good description of the entire spin-wave dispersion, with $SJ_\parallel = 9.6 \pm 0.1$ meV and $SJ_\perp = 2.9 \pm 0.1$ meV for $x = 0.40$, and $SJ_\parallel = 9.3 \pm 0.1$ meV and $SJ_\perp = 5.7 \pm 0.2$ meV for $x = 0.35$. The relative dispersion of the optic mode along $(h, 0)$ with respect to the acoustic mode can be accounted for by a small second-neighbor interaction $SJ_{a,0,a} \approx -0.8$ meV connecting the two planes of a bilayer along $[a, 0, a]$ in the real-space lattice. (In the same notation $J_\parallel$ is $J_{a,0,0}$ and $J_\perp$ is $J_{0,0,a}$.) The corresponding dispersion relations are shown by the dotted lines in Fig. 2. The other second-neighbor interactions, $J_{a,a,0}$ and $J_{2a,0,0}$, do not improve the fit, and $J_{a,a,a}$, which yields a similar improvement as $J_{a,0,a}$, we dismissed as it requires a carrier to make *three* hops along Mn-O-Mn bonds and so is expected to be weaker still. We note that our values of $SJ_\parallel$ and $SJ_\perp$ for $x = 0.40$ agree well with reports from other groups [6,7], but that those data were confined to $\hbar\omega \leq 25$ meV, and were therefore unable to test the applicability of the nnHFM model.

The spin-wave dispersion for the DE model is precisely that for the nnHFM in the $J_H = \infty$ RPA limit [16,17]. Treatment to second order in a $1/S$ expansion for the 2D DE model (but still $J_H = \infty$ for one band) [18] yields a reduction of ~50% in stiffness D (defined by $\hbar\omega = Dq^2$ in the small q limit), but in fact $\hbar\omega$ at $q = (1/2, 0)$ is 10%–20% greater than for the nnHFM with that reduced D (Ref. [18], Fig. 1). A similar reduction of 35% in energy scale, and a small hardening towards zone boundary, was found in 3D for $x = 0.30$ using a variational approach that further allowed for finite $J_H = W/2$ [19]. Data from band structure calculations (majority carrier full bandwidth $W \approx 2$–3 eV) [20] together with results from the $1/S$ expansion yield $\hbar\omega(1/2, 0) \approx 20$–$40$ meV, in good quantitative agreement with our data. Remarkably, a simple one-band DE model provides an explanation for both the energy scale and near-nnHFM dispersion relation.

For comparison with our data for $x = 0.30$, we calculated the spin-wave stiffness and optic gap from the fitted

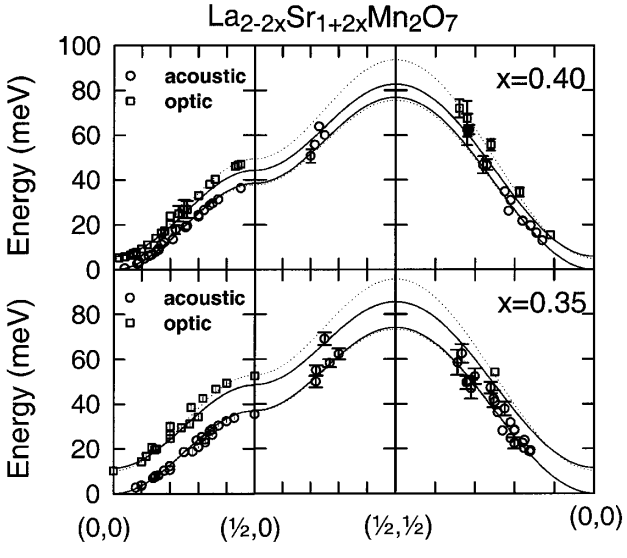

FIG. 2. Measured spin-wave dispersion relations for $x = 0.40$, $x = 0.35$. Solid lines show the best fits to the nnHFM model (parameters in text). Dashed lines show the best fit including diagonal exchange as described in the text. (For $x = 0.40$, $SJ_\parallel = 10.3 \pm 0.1$, $SJ_\perp = 5.8 \pm 0.5$, $SJ_{a,0,a} = -0.8 \pm 0.1$ meV; for $x = 0.35$, $SJ_\parallel = 9.9 \pm 0.2$, $SJ_\perp = 8.1 \pm 0.7$, $SJ_{a,0,a} = -0.8 \pm 0.2$ meV.) Error bars are omitted if smaller than the markers.

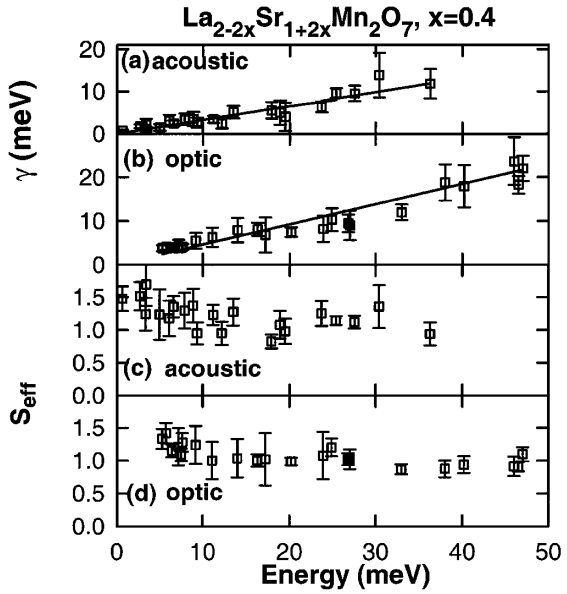

FIG. 3. Energy dependence for $x = 0.40$ of the inverse spin wave lifetime γ for (a) acoustic (b) optic spin waves, and of the spin-wave intensity $S_{\rm eff}$ in the scattering cross section for the nnHFM model (see text) for (c) acoustic (d) optic spin waves. Error bars are omitted if smaller than the markers.

exchange constants, and used the small q limits of the dispersion relations for the nnHFM to obtain effective nearest-neighbor exchange constants $SJ_{\parallel}^{\rm eff}$ and $SJ_{\perp}^{\rm eff}$. For $x = 0.30$, only long wavelength data were taken, which are necessarily insensitive to further neighbor interactions, and $SJ_{\parallel}^{\rm eff}$ and $SJ_{\perp}^{\rm eff}$ are the result of fits directly to the counts. The results are summarized in Fig. 4(a). $SJ_{\parallel}^{\rm eff}$ is only weakly dependent on the hole doping x, and is very similar to values obtained in the 3D manganites [21–26]. In contrast, $SJ_{\perp}^{\rm eff}$ is remarkably sensitive to the hole doping, with $J_{\perp}^{\rm eff}/J_{\parallel}^{\rm eff}$ changing from 1.1 to 0.25 over the range $x = 0.30$–0.40. In the bilayer manganites, delocalization

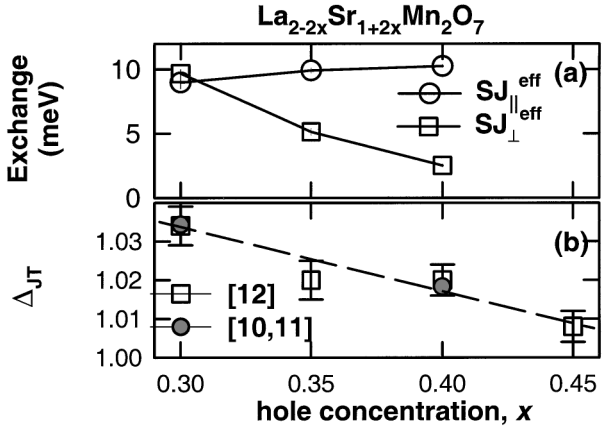

FIG. 4. (a) $SJ_{\parallel}^{\rm eff}$ and $SJ_{\perp}^{\rm eff}$ for the nnHFM model derived from the spin-wave stiffness and optic gap. (b) Distortion of the MnO_6 octahedra, where $\Delta_{\rm JT} = (1/2)(d_{\rm Mn\text{-}O(1)} + d_{\rm Mn\text{-}O(2)})/d_{\rm Mn\text{-}O(3)}$. Error bars are omitted if smaller than the markers.

of the carriers in two dimensions is expected to stabilize planar $d_{x^2-y^2}$ orbital ordering, even with elongation of the MnO_6 octahedra perpendicular to the planes [27]. Ferromagnetic exchange between the planes arises from overlap of O p_z and Mn $d_{3z^2-r^2}$ orbitals, whereas ferromagnetic exchange in a plane is due to overlap of O p_x or O p_y and Mn $d_{x^2-y^2}$ orbitals (Fig. 1). Increasing $SJ_{\perp}^{\rm eff}$, but almost constant $SJ_{\parallel}^{\rm eff}$, therefore directly implies increasing $d_{3z^2-r^2}$ orbital occupancy, with little change in $d_{x^2-y^2}$ occupancy, as the hole doping decreases or equivalently as the number of e_g electrons increases. Diffraction studies [10–12] show that the MnO_6 octahedra elongate significantly as the hole doping is reduced, as reflected in the increasing ratio of the mean apical to equatorial Mn-O bond lengths, Δ_{JT} [Fig. 4(b)]. This observation led to the proposal of shifting orbital polarization [12], as elongation is expected to lower the energy of the $d_{3z^2-r^2}$ orbital with respect to the $d_{x^2-y^2}$ orbital. Until now, only indirect evidence in support of this idea has come from anisotropic magnetostriction [28] and optical conductivity data [29]. Our measurements of the interplane exchange directly demonstrates the hypothesis, and show that the change is almost entirely in the $d_{3z^2-r^2}$ orbital occupancy.

We now turn to the lifetime of the spin waves. Figure 3(a) shows γ as a function of excitation energy $\hbar\omega$ along $(h, 0)$ for $x = 0.40$. For both the acoustic and optic modes, γ increases approximately linearly with $\hbar\omega$ to the zone boundary, with the damping a large fraction of the excitation energy $-\gamma(q)/\hbar\omega(q) = 0.33 \pm 0.02$ and 0.46 ± 0.02 for the acoustic and optic modes, respectively. In particular, there is no steep increase where the spin-wave branch crosses an optic phonon mode at $\approx$20 meV [29]. (Note there is a small deviation of the lowest energy optic modes from the linear relation: at the zone center we found $\gamma = 3.8 \pm 0.7$ meV, the same as 4.0 ± 0.2 meV in [7].) We observed similar behavior—linear $\gamma(q)/\hbar\omega(q)$ to the zone boundary for both acoustic and optic modes—for $x = 0.35$ [$\gamma(q)/\hbar\omega(q) = 0.24 \pm 0.01$ and 0.38 ± 0.01, respectively]. The important aspects of the data are that the slopes are of order unity, and that γ is much larger than $k_B T \approx 1$ meV throughout most of the Brillouin zone. Spin-wave broadening can arise from static or dynamical fluctuations. The first would translate into quenched disorder which would cause the exchange constants to belong to distributions of width $\Delta J_{\parallel}$ and $\Delta J_{\perp}$, immediately leading to decay rates $\gamma(q) = \Delta\hbar\omega(q)$. Because the measured slopes $\gamma(q)/\hbar\omega(q)$ are of order unity, this would imply site to site fluctuations in J of order J itself, something which might well yield carrier localization, in contradiction with the low temperature metallicity of our samples. This leaves us to consider dynamical damping mechanisms, although we do not exclude a small static contribution to $\gamma(q)/\hbar\omega(q)$. There are several possible channels: (i) magnon-magnon scattering, (ii) magnon-phonon coupling, (iii) coupled orbital-lattice fluctuations, and (iv) magnon-electron scattering. Case (i) has not been considered for DE, but experiment and theory for the

planar nnHFM suggest that it is unlikely to explain the heavy damping. K_2CuF_4 provides an excellent realization of the planar nnHFM for $S = 1/2$, and nowhere in the Brillouin zone was $\gamma(q)/\hbar\omega(q)$ found to exceed 0.02 for $T/J < 0.25$ [30]. For $q \to 0$ the leading order term for γ is linear in $\hbar\omega$, $\gamma(q)/\hbar\omega(q) = (1/2\pi)(T/JS^2)^2$ [31], which when evaluated at $T = 10$ K with $SJ_{\parallel}^{\text{eff}}$ and $S = (4 - x)/2$ yields $\approx 1.6 \times 10^{-3}$, ~ 100 times smaller than our measurements. Case (ii), magnon-phonon coupling, may dampen the spin waves without softening the dispersion [32]. Significant broadening at optic phonon frequencies has been observed in $La_{0.7}Ca_{0.3}MnO_3$ [22]. However, no step in γ is observed in our data, indicating that another mechanism must be sought [33]. The effect of (iii), coupled orbital-lattice fluctuations, softening the spin-wave branch near the zone boundary has been treated quantitatively [34], but the effect on spin-wave damping has not been considered. However, the absence of softening of the spin-wave modes suggests that the mechanism is probably unimportant. Golosov considered case (iv), magnon-electron scattering, at $T = 0$ for DE [18]. Figure 1 of Ref. [18] yields $\gamma(1/2, 0)/\hbar\omega(1/2, 0) = 1\text{–}4 \times 10^{-2}$ for the x considered, ~ 10 times too small, but elsewhere on the zone boundary $\gamma/\hbar\omega$ can reach 0.15. This magnitude and the sensitivity of $\gamma(q)$ to precise details of the band structure suggest the plausibility of the mechanism to explain our results. Numerical simulations in 1D [35] support this conclusion. Furukawa [36] has pointed out the existence of a strongly T-dependent magnon-electron contribution to γ, which is also linear in ω, as we have observed. However, this contribution vanishes in the $T \to 0$ limit.

Finally, we consider the absolute value of the scattering cross section. Figures 3(c)–3(d) show that S_{eff} is nearly constant along $(h, 0)$ for $x = 0.4$, and $x = 0.35$ shows similar behavior. $S_{\text{eff}}(q)$ is constant for the nnHFM, with deviations less than 5% from the nnHFM value for the DE model [19]. Our value of $S_{\text{eff}} = 1.0\text{–}1.2$ for both $x = 0.35$ and 0.40 is somewhat smaller than $(4 - x)/2 \approx 1.8$. However, systematic error arising from the normalization by vanadium standard can easily be 30%. We have $S_{\text{eff}} = 1.7 \pm 0.2$ for $x = 0.30$.

In summary, we have measured the doping-dependent spin waves in a two-dimensional manganite. The three major findings are (i) the strong doping dependence of the interplane (but intrabilayer) magnetic exchange, which directly demonstrates the preferential filling of the $d_{3z^2-r^2}$ band with decreasing hole concentration, (ii) the low-temperature spin-wave dispersion in the ferromagnetic bilayers of $La_{2-2x}Sr_{1+2x}Mn_2O_7$, $x = 0.35\text{–}0.40$ can be understood entirely within the double exchange picture, and (iii) the anomalously large low-temperature spin-wave damping, which rises linearly with spin-wave energy, and contains no special resonances where the damping might be enhanced due to crossing of other excitation branches such as phonons or orbitons.

[1] H. Kuwahara *et al.,* Science **270**, 961 (1995); A. Asamitsu *et al.,* Nature (London) **388**, 50 (1997); K. Miyano *et al.,* Phys. Rev. Lett. **78**, 4257 (1997); J-S. Zhou *et al.,* Phys. Rev. Lett. **79**, 3234 (1997).

[2] C. Zener, Phys. Rev. **82**, 403 (1951).

[3] P. W. Anderson and H. Hasegawa, Phys. Rev. **100**, 675 (1955).

[4] A. J. Millis, Nature (London) **392**, 147 (1998).

[5] Y. Moritomo *et al.,* Nature (London) **380**, 141 (1996); T. Kimura *et al.,* Science **274**, 1698 (1996).

[6] H. Fujioka *et al.,* J. Phys. Chem. Solids **60**, 1165 (1999); unpublished data at long wavelengths for $x = 0.3\text{–}0.5$ are presented in K. Hirota *et al.,* cond-mat/0104535.

[7] T. Chatterji *et al.,* Phys. Rev. B **60**, 6965 (1999).

[8] G. Chaboussant *et al.,* Physica (Amsterdam) **276B–278B**, 801 (2000).

[9] T. G. Perring *et al.,* Phys. Rev. B **58**, R14 693 (1998).

[10] D. N. Argyriou *et al.,* Phys. Rev. B **59**, 8695 (1999).

[11] J. F. Mitchell *et al.,* Phys. Rev. B **55**, 63 (1997).

[12] M. Kubota *et al.,* J. Phys. Soc. Jpn. **69**, 1606 (2000).

[13] T. Chatterji *et al.,* Europhys. Lett. **46**, 801 (1999); S. Rosenkranz *et al.,* J. Appl. Phys. **87**, 5816 (2000).

[14] G. Aeppli, S. M. Hayden, and T. G. Perring, Phys. World **10**, 33–37 (1997).

[15] S. W. Lovesey, *Theory of Neutron Scattering from Condensed Matter* (Oxford University Press, Oxford, 1984).

[16] N. Furukawa, J. Phys. Soc. Jpn. **65**, 1174 (1996).

[17] X. Wang, Phys. Rev. B **57**, 7427 (1998).

[18] D. I. Golosov, Phys. Rev. Lett. **84**, 3974 (2000).

[19] P. Wurth and E. Müller-Hartmann, Eur. Phys. J. B **5**, 403 (1998); renormalization was first seen numerically in 1D chains: T. A. Kaplan and S. D. Mahanti, J. Phys. Condens. Matter **9**, L291 (1997); *Physics of Manganites,* edited by T. A. Kaplan and S. D. Mahanti (Kluwer, New York, 1999), p. 135.

[20] X. Y. Huang *et al.,* Phys. Rev. B **62**, 13 318 (2000).

[21] T. G. Perring *et al.,* Phys. Rev. Lett. **77**, 711 (1996).

[22] P. Dai *et al.,* Phys. Rev. B **61**, 9553 (2000).

[23] H. Y. Hwang *et al.,* Phys. Rev. Lett. **80**, 1316 (1998).

[24] J. A. Fernandez-Baca *et al.,* Phys. Rev. Lett. **80**, 4012 (1998).

[25] M. C. Martin *et al.,* Phys. Rev. B **53**, 14 285 (1996).

[26] There is no simple relationship between the spin-wave stiffness D and T_C or T_N, as the latter depends on the very weak interlayer coupling as well as $J_{\parallel}$ and $J_{\perp}$.

[27] R. Maezono and N. Nagaosa, Phys. Rev. B **61**, 1825 (2000).

[28] T. Kimura *et al.,* Phys. Rev. Lett. **81**, 5920 (1998).

[29] T. Ishikawa *et al.,* Phys. Rev. B **62**, 12 354 (2000).

[30] K. Hirakawa *et al.,* J. Phys. Soc. Jpn. **52**, 4220 (1983).

[31] P. Kopietz and G. Castilla, Phys. Rev. B **43**, 11 100 (1991).

[32] N. Furukawa, J. Phys. Soc. Jpn. **68**, 2522 (1999).

[33] N. Furukawa and K. Hirota [Physica (Amsterdam) **291B**, 324 (2000)] claim to observe damping due to magnon-phonon coupling. However, no quantitative analysis is presented.

[34] G. Khaliullin and R. Kilian, Phys. Rev. B **61**, 3494 (2000).

[35] T. A. Kaplan *et al.,* Phys. Rev. Lett. **86**, 3634 (2001).

[36] N. Furukawa, Physica (Amsterdam) **237B–238B**, 71 (1997); N. Furukawa and K. Hirota, *ibid.* **241B–243B**, 780 (1998).